Generation and characterization of neutralizing antibodies against M1R and B6R proteins of monkeypox virus

Yuanyuan Qu[1,8], Wanbo Tai [1,8], Enhao Ma[2,3,4,8], Qiwei Jiang[5,8], Miao Fan[6], Wangcheng Xiao[1], Chongyu Tian[1], Yang Liu[1], Jianying Liu[1], Xinquan Wang [7], Jiwan Ge [6] ✉ & Gong Cheng [2,3,4] ✉

The global outbreak of monkeypox virus (MPXV), combined with the termination of smallpox vaccination and the lack of specific antiviral treatments, raises increasing concerns. The surface proteins M1R and B6R of MPXV are crucial for virus transmission and serve as key targets for vaccine development. In this study, a panel of human antibodies targeting M1R and B6R is isolated from a human antibody library using phage display technology. Among these antibodies, A138 against M1R and B026 against B6R show the most potent broad-spectrum neutralizing activities against MPXV and Vaccinia virus (VACV). When used in combination, A138 and B026 exhibit complementary neutralizing activity against both viruses in vitro. X-ray crystallography reveals that A138 binds to the loop regions of M1R, similar to the vulnerable epitope of 7D11 on VACV L1R. By contrast, A129 targets a more cryptic epitope, primarily comprising the β-strands of M1R. Moreover, prophylactic and therapeutic administration of A138 or B026 alone provides partial protection, while combining these two antibodies results in enhanced protection against VACV in male C57BL/6 mice. This study demonstrates of a dual-targeting strategy using two different components of the virion for the prevention and treatment of MPXV infection.

Monkeypox virus (MPXV) a member of the genus Orthopoxvirus and is primarily restricted to rural tropical rainforest areas of West and Central Africa[1]. Individuals typically acquire infection through direct or indirect contact with infected animals[1–3]. MPXV has raised concerns due to the increasing number of cases in Africa over the past 20 years and unprecedented outbreaks in non-endemic regions[3]. Since the sudden outbreak in 2022[4,5], MPXV has spread to 127 countries and regions worldwide, with 117663 laboratory-confirmed cases as of

[1]Institute of Infectious Diseases, Shenzhen Bay Laboratory, Shenzhen, Guangdong 518132, China. [2]New Cornerstone Science Laboratory, Tsinghua University-Peking University Joint Center for Life Sciences, School of Basic Medical Sciences, Tsinghua University, Beijing 100084, China. [3]Institute of Pathogenic Organisms, Shenzhen Center for Disease Control and Prevention, Shenzhen 518055, China. [4]Southwest United Graduate School, Kunming 650092, China. [5]Changchun Veterinary Research Institute, Chinese Academy of Agricultural Sciences, State Key Laboratory of Pathogen and Biosecurity, Key Laboratory of Jilin Province for Zoonosis Prevention and Control, Changchun, China. [6]Key Laboratory of Pathogen Infection Prevention and Control (MOE), State Key Laboratory of Respiratory Health and Multimorbidity, National Institute of Pathogen Biology, Chinese Academy of Medical Sciences & Peking Union Medical College, Beijing 102629, China. [7]The Ministry of Education Key Laboratory of Protein Science, Beijing Advanced Innovation Center for Structural Biology, Beijing Frontier Research Center for Biological Structure, Collaborative Innovation Center for Biotherapy, School of Life Sciences, Tsinghua University, Beijing 100084, China. [8]These authors contributed equally: Yuanyuan Qu, Wanbo Tai, Enhao Ma, Qiwei Jiang. ✉e-mail: gejiwan@ipbcams.ac.cn; gongcheng@mail.tsinghua.edu.cn

December, 2024[6]. Most cases were reported in men who have sex with men and those who have been in direct contact with symptomatic or asymptomatic patients[7,8]. Compared to previous outbreaks, the current epidemic strain of MPXV appears to spread faster and skin lesions seem to be more limited in distribution[3]. The outbreaks in 2022 were caused by clade IIb (or West African clade) of the MPXV, with a low case fatality ratio of less than 1%[9–11]. Notably, the 2022 MPXV differs from the related 2018–2019 strains by an average of 50 single-nucleotide polymorphisms[12], implying a considerably higher mutation rate (roughly 6- to 12-fold) than previous estimates for Orthopoxviruses (1–2 substitutions per genome per year)[13]. Three amino acid changes (D209N, P722S, and M1741I) occurred in the key antibody target surface glycoprotein B21[14]. However, it remains unclear whether and how these genetic variations drive the epidemiological phenotype. Currently, the non-synonymous single nucleotide polymorphisms on immunogenic surface glycoprotein[14,15], the waning smallpox immunity in the general population, and the termination of smallpox vaccination[16] are considered to be the main reasons for the immune evasion and accelerated transmission of MPXV.

Antibodies play a critical role in providing immunity against Orthopoxviruses[17], and previous studies have shown that polyclonal antibodies are effective in providing protection against lethal challenges with MPXV or vaccinia virus (VACV) in non-human primates and mice[18]. Vaccinia immune globulin, derived from antiserum elicited by vaccinia vaccine, is an approved treatment for complications associated with smallpox vaccination. However, its use is limited by availability, low specific activity, and the risk of contamination with blood-borne infectious agents. Therefore, there is an urgent need for the development of protective antibodies for the prevention and treatment of MPXV infections. However, the complex proteome of Orthopoxviruses, as well as the diversity of viral particles, including mature virions (MV) or enveloped virions (EV)[19], poses challenges in definitively identifying suitable antigens for the development of therapeutic antibodies.

Currently, the majority of available neutralizing antibodies developed against Orthopoxviruses have been developed based on VACV antigens, with only a few antibodies against MPXV antigens[20–22]. Previous studies using mouse models of VACV infection have identified several surface proteins of MV and EV as targets for neutralizing and protective antibodies, including A27L, L1R, H3L, D8L, A28L, A13L, and A17L for MV, as well as B5R and A33R for EV[19]. Six principal antibodies essential for cross-neutralization and protection against infection with four Orthopoxvirus species have also been identified, targeting various VACV antigens such as D8L, H3L, A27L, L1R for MV, as well as B5R and A33R for EV. Investigations into various human mAb formulations suggest that the incorporation of antibodies targeting both MV and EV antigens is crucial for providing adequate protection against Orthopoxvirus challenge in animals[23]. Additionally, studies on multicomponent mRNA vaccine candidates against MPXV have demonstrated that vaccine formulations containing M1R and B6R exhibit superior efficacy in eliciting neutralizing and protective antibodies rather than those without M1R and B6R[24,25]. In summary, although numerous antigens have been identified as neutralization targets in Orthopoxviruses, the surface antigens consistently included in subunit vaccines are L1R/M1R for MV and B5R/B6R for EV. Therefore, we primarily focused on M1R on the surface of MV and B6R on the surface of EV for screening and isolation of neutralizing antibodies against MPXV.

In this work, we employed phage display technology to generate a large panel of MPXV-specific human antibodies targeting M1R and B6R, after which we evaluated their binding and neutralizing activity. We also examined the cross-reactivity of individual antibody administration, two-antibody combinations and bispecific antibodies (bsAbs) against both VACV and MPXV in vitro. Our findings revealed that among the antibodies generated in this study, the combined use of two antibodies targeting two different MPXV antigens or their corresponding bsAbs exhibited superior neutralizing activity compared to the single antibodies targeting M1R or B6R alone. Furthermore, we defined the binding epitopes of M1R and B6R antibodies through X-ray crystallography and biochemical analyzes. Our results demonstrated that A138 binds to M1R at an epitope similar to that of the previously reported mouse antibody 7D11[26] targeting VACV L1R, whereas A129 binds to a previously unreported epitope. Additionally, the B6R antibody B026 binds to the stalk region of B6R, while B019 primarily binds to domain 4 of B6R. Lastly, we evaluated the prophylactic and therapeutic effects of single antibodies and antibody combinations in mouse models of VACV and MPXV infection. In agreement with our in vitro neutralization assays, the two-antibody combination exhibited a more potent protective effect than single antibodies. Taken together, our findings suggest that a dual-targeting strategy utilizing two different components of MPXV antigens, M1R and B6R, may offer a promising approach for the prevention and treatment of MPXV infection.

Results
Isolation and characterization of antibodies targeting MPXV M1R and B6R

In this study, we employed phage surface display technology to identify a diverse and extensive array of antibodies targeting M1R and B6R proteins on the surface of MPXV (Fig. 1A). The M1R and B6R antibodies were isolated from a fully human antibody library (ST-ST-HuNAL, Fab format, Sanyou Bio), which was constructed using peripheral blood mononuclear cells (PBMCs) derived from more than 2000 healthy donors aged between 20 and 60 years. To isolate the target antibodies, we adopted a standard solid-phase immuno tube screening strategy (Fig. S1). The recombinant M1R or B6R proteins were used as bait, and three rounds of panning were conducted (Fig. S1 and Table S1), which respectively yielded 37 and 40 clones (Table S2), each exhibiting unique sequences. Subsequently, we sequenced the V regions and assessed the length of complementarity-determining region 3 (CDR3). Notably, IGHV3-23, IGHV3-30, IGHV3-66 and IGHV3-21, as well as IGKV1-12 and IGKV1-39, were found to be significantly prevalent among the M1R binding antibodies (Fig. 1B). Similarly, antibodies targeting B6R also exhibited high frequencies in the IGHV3-23, IGHV3-30, IGKV1-12, and IGKV1-39 germlines (Fig. 1C). Further analysis of the CDR3 length in these binding antibodies revealed values within the range of 8-10 amino acids. While the antibodies targeting B6R and M1R shared a similar average CDRH3 length, a higher number of B6R antibodies were found to possess longer CDRH3 compared to M1R antibodies (Fig. 1D). Finally, we extracted plasmid DNA containing the coding sequences of the identified human antibodies and constructed full-length IgG1 constructs expression in Expi239F system.

We then assessed the binding and neutralizing activity of the antibodies using enzyme-linked immunosorbent assay (ELISA) and plaque reduction neutralization test (PRNT), respectively (Figs. 1E and S2). Overall, M1R antibodies showed slightly weaker binding affinities compared to B6R antibodies. Only a few M1R antibodies demonstrated remarkable binding affinity, with half-maximal effective concentration (EC$_{50}$) values below 1 ng/mL, including A046, A084 and A094, while the remaining antibodies displayed much lower binding activities with EC$_{50}$ values above 20 ng/mL. By contrast, B6R antibodies showed robust binding activity, with the majority of clones exhibiting EC$_{50}$ values below 10 ng/mL. Notably, B026, B046, B089, B161 and B177 exhibited particularly tight binding to B6R, with EC$_{50}$ values below 0.5 ng/mL (Fig. 1E). We further evaluated the in vitro neutralization capacity of M1R and B6R antibodies against replication-deficient MPXV[27]. Specifically, MV forms of MPXV were utilized to evaluate the neutralization potency of M1R antibodies, while EV forms were employed to assess the neutralizing capacity of B6R antibodies. The potency of neutralization was determined using the half-maximal
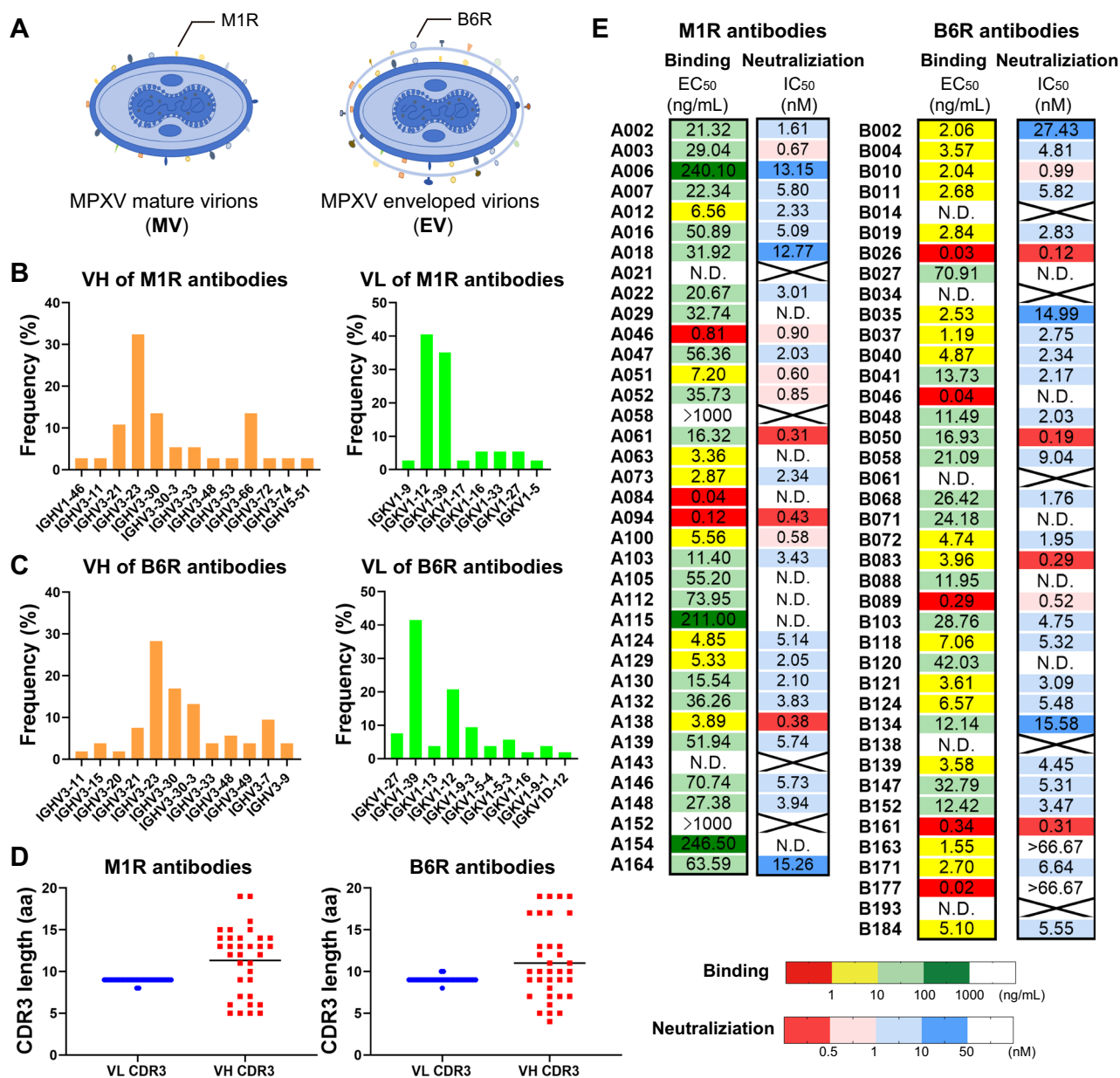
A

MPXV mature virions (**MV**) — M1R

MPXV enveloped virions (**EV**) — B6R

B VH of M1R antibodies / VL of M1R antibodies

C VH of B6R antibodies / VL of B6R antibodies

D M1R antibodies / B6R antibodies (CDR3 length (aa): VL CDR3, VH CDR3)

E

	M1R antibodies			B6R antibodies	
	Binding EC$_{50}$ (ng/mL)	Neutraliziation IC$_{50}$ (nM)		Binding EC$_{50}$ (ng/mL)	Neutraliziation IC$_{50}$ (nM)
A002	21.32	1.61	B002	2.06	27.43
A003	29.04	0.67	B004	3.57	4.81
A006	240.10	13.15	B010	2.04	0.99
A007	22.34	5.80	B011	2.68	5.82
A012	6.56	2.33	B014	N.D.	
A016	50.89	5.09	B019	2.84	2.83
A018	31.92	12.77	B026	0.03	0.12
A021	N.D.	X	B027	70.91	N.D.
A022	20.67	3.01	B034	N.D.	
A029	32.74	N.D.	B035	2.53	14.99
A046	0.81	0.90	B037	1.19	2.75
A047	56.36	2.03	B040	4.87	2.34
A051	7.20	0.60	B041	13.73	2.17
A052	35.73	0.85	B046	0.04	N.D.
A058	>1000	X	B048	11.49	2.03
A061	16.32	0.31	B050	16.93	0.19
A063	3.36	N.D.	B058	21.09	9.04
A073	2.87	2.34	B061	N.D.	X
A084	0.04	N.D.	B068	26.42	1.76
A094	0.12	0.43	B071	24.18	N.D.
A100	5.56	0.58	B072	4.74	1.95
A103	11.40	3.43	B083	3.96	0.29
A105	55.20	N.D.	B088	11.95	N.D.
A112	73.95	N.D.	B089	0.29	0.52
A115	211.00	N.D.	B103	28.76	4.75
A124	4.85	5.14	B118	7.06	5.32
A129	5.33	2.05	B120	42.03	N.D.
A130	15.54	2.10	B121	3.61	3.09
A132	36.26	3.83	B124	6.57	5.48
A138	3.89	0.38	B134	12.14	15.58
A139	51.94	5.74	B138	N.D.	X
A143	N.D.	X	B139	3.58	4.45
A146	70.74	5.73	B147	32.79	5.31
A148	27.38	3.94	B152	12.42	3.47
A152	>1000	X	B161	0.34	0.31
A154	246.50	N.D.	B163	1.55	>66.67
A164	63.59	15.26	B171	2.70	6.64
			B177	0.02	>66.67
			B193	N.D.	X
			B184	5.10	5.55

Binding — 1, 10, 100, 1000 (ng/mL)

Neutraliziation — 0.5, 1, 10, 50 (nM)

Fig. 1 | Isolation and characterization of the M1R and B6R antibodies. A Diagram of the EV and MV forms of MPXV. M1R and B6R are located on the surface of the mature and enveloped virions, respectively. **B** and **C** Frequency distribution of human IGVH and IGVL in M1R (**B**) and B6R antibodies (**C**). **D** The length of the CDR3 at IGVH and IGVL in M1R and B6R antibodies. (**E**) Binding activity and neutralization potency of the M1R and B6R antibodies. The binding assay was based on ELISA while the neutralizing activity was measured using replication-deficient MPXV. The number in the box indicates the half-maximal effective concentration (EC$_{50}$) or half-maximal inhibitory concentration (IC$_{50}$) values. Blank or excluded values were represent by an X in the corresponding table cells. No detective (N.D.) indicates that no response was observed at the highest concentration, while > 1000 or > 66.7 denotes that the EC50 or IC50 value of the antibody is higher than the maximum detectable concentration. Binding and neutralization curves are shown in Figure S2. Source data are provided as a Source Data file.

---

inhibitory concentration (IC$_{50}$). The IC$_{50}$ values of most antibodies were above 1 nM, but three M1R antibodies (A061, A094, and A138) and four B6R (B026, B050, B083, and B161) antibodies demonstrated more potent neutralizing activity, with IC$_{50}$ values below 0.5 nM. Notably, M1R antibody A138 and B6R antibody B026 stood out with the most potent neutralization activity (Fig. 1E).

To map out the epitopes of these antibodies, we performed a cross-competition assay using Bio-Layer Interferometry (BLI) (Fig. S3). Our findings revealed a spectrum of epitopes utilized by the tested antibodies. Notably, some of these epitopes overlapped with those recognized by previously reported antibodies, such as 7D11[26] targeting M1R and 8AH8AL[28] targeting B6R. However, we also identified antibodies binding to novel epitopes that have not yet been characterized.

M1R and B6R antibodies exhibited cross-neutralization activity against VACV and MPXV
Next, we evaluated the neutralizing activities of M1R and B6R antibodies against VACV and replication-deficient MPXV. Four antibodies (A138 and A129 against M1R, B026 and B019 against B6R) were chosen for the following cross-neutralization experiments considering their high expression level, differentiated neutralizing activity and varied binding epitopes. Here, we prepared EV and MV forms of VACV and
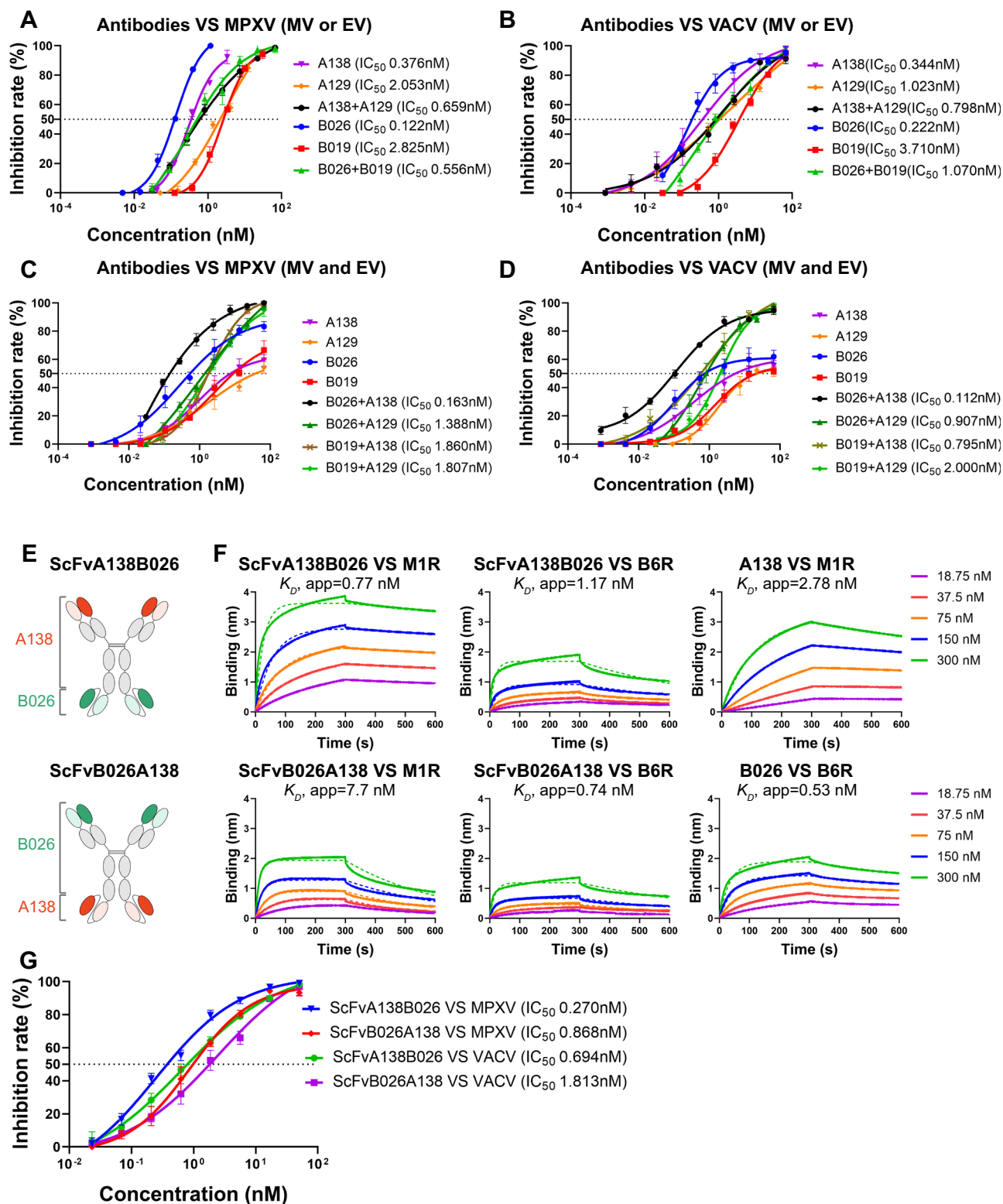
replication-deficient MPXV for the neutralization assays with M1R and B6R antibodies (Fig. 2A, B). Conversely, when assessed the combination of antibodies targeting different antigens, a mixture of EV and MV forms of VACV/MPXV was used (Fig. 2C, D).

The results suggested that M1R antibodies could effectively neutralize the MV form of the virus but not the EV form (Fig. S4). Conversely, the B6R antibodies demonstrated neutralization of the EV but not the MV form of MPXV (Fig. S4). The neutralizing activity of A138 or A129 against MPXV and VACV was comparable (Fig. 2A, B), in

agreement with previous reports on the 7D11 antibody[29,30]. Similarly, the B6R antibodies B026 and B019 also exhibited a comparable neutralizing capacity against MPXV and VACV (Fig. 2A, B). However, compared to B019, B026 exhibited stronger neutralizing activity against both MPXV and VACV (Fig. 2A, B). Furthermore, we explored the combined effect of two antibodies targeting the same antigens against VACV and replication-deficient MPXV. The results suggested that mixing two antibodies (A129 + A138 or B019 + B026) led to no obvious enhancement of the neutralizing effect (Fig. 2A, B).

Fig. 2 | Cross-neutralizing potency of M1R and B6R antibodies against VACV and replication-deficient MPXV. A, B Neutralizing activity of individual antibodies (A129, A138, B026, and B019) or antibody cocktail targeting the same antigens against MV and EV forms of replication-deficient MPXV (**A**) and VACV (**B**). MVs of MPXV were utilized to evaluate the neutralization potency of M1R antibodies, while EVs were employed to assess the neutralizing capacity of B6R antibodies.
C, D Neutralization activity of individual antibodies (A129, A138, B026, and B019) or antibody cocktail targeting the two different antigens against a mixture of MV and EV forms of replication-deficient MPXV (**C**) or VACV (**D**). **E** Schematic of bispecific antibodies (bsAbs). The parental mAbs contributing to the bsAbs are color-coded: red A138 and green B026. **F** Binding affinity of bsAbs for M1R and B6R. M1R and B6R were immobilized on the surface of biosensors and individual antibodies were tested at various concentrations. The association and dissociation of antibodies is indicated by the dashed line, which represents the fitted curve. The apparent dissociation constants (K_D, app) are shown above each plot. **G** Cross-neutralizing activity of bsAbs against VACV and replication-deficient MPXV. Data from a representative neutralization experiment are shown for each antibody. The experiment was replicated twice with similar results. The data represent means ± SEM of triplicates indicated by error bars. The dashed line indicates a 50% reduction of viral infectivity. Source data are provided as a Source Data file.

Additionally, we conducted assessments on the neutralizing activities of M1R and B6R antibody combinations using a mixture of MV and EV forms of MPXV/VACV (Fig. 2C, D). Notably, none of the individual M1R or B6R antibodies could entirely neutralize the combination of MV and EV of MPXV/VACV, even at the maximum concentration of 66.7 nM (10 µg/mL). However, the four combinations of M1R and B6R antibodies exhibited potent neutralizing activity, successfully neutralizing the mixture of MV and EV in both MPXV (Fig. 2C) and VACV (Fig. 2D). Among these combinations, the pairing of A138 and B026 exhibited the most robust neutralizing activity against MPXV and VACV, with IC_{50} values of 0.163 and 0.112 nM, respectively. Therefore, the neutralization and cross-neutralization of MPXV and VACV can be more effectively achieved by employing a combination of two antibodies targeting different antigens, rather than relying solely on a single antibody with a specific neutralization target.

Design and characterization of bispecific antibodies
To further increase the neutralizing potency and broaden the spectrum against MPXV and other Orthopoxviruses, we designed and synthesized seven bispecific antibodies (bsAbs) in IgG-ScFv format[31], Bs(ScFv) format, DSD format[32] and Cross-Ab format[33] based on A138 and B026 (Figs. 2E and S5). All the bsAbs were successfully obtained as determined by sodium dodecyl-sulfate polyacrylamide gel electrophoresis (SDS-PAGE) analysis (Fig. S5). We evaluated the binding affinity of these bsAbs for M1R and B6R using BLI. Differentiated binding patterns were found in various forms of bsAbs (Figs. 2F and S5). Notably, ScFvA138B026 and ScFvB026A138 displayed robust binding to both M1R and B6R, whereas the remaining bsAbs exhibited lower or undetectable affinity (Figs. 2F and S5). The binding affinity of ScFvA138B026 for M1R and B6R were determined to be 0.77 and 1.17 nM, respectively. For ScFvB026A138, the K_D values were 7.7 and 0.74 nM for binding to M1R and B6R, respectively. Remarkably, the binding capacity of ScFvA138B026 and ScFvB026A138 was comparable to that of their parental antibodies (K_D = 2.78 nM for A138 and M1R; K_D = 0.53 nM for B026 and B6R) (Figs. 2F and. S5).

Next, we further assessed the neutralizing efficacy of the these two bsAbs in IgG-ScFv format (ScFvA138B026 and ScFvB026A138) against VACV and replication-deficient MPXV. Interestingly, ScFvA138B026 demonstrated slightly superior neutralization compared to ScFvB026A138, with IC_{50} concentrations of 0.270 nM and 0.694 nM (IC_{50}) for MPXV and VACV, respectively (Fig. 2G). The enhanced neutralizing activity of ScFvA138B026 might be attributed to its stronger binding affinity for M1R and B6R. Despite the marginally lower neutralizing efficacy of ScFvA138B026 compared to the mixture of parental antibodies, it exhibited significantly better neutralization effects than B026 or A138 against MPXV and VACV (Fig. 2C, D, G).

Structural basis for the recognition of M1R by the antibodies
To gain insights into the molecular mechanism underlying the neutralization activity of M1R antibodies, we attempted a structural study on the M1R-A129/A138 Fab complexes. The crystal structures of the M1R-A129/A138 Fab complexes were determined at resolutions of 2.17

and 3.49 Å, respectively (Fig. 3, Table 1 and Fig. S8). The binding approach of A138 Fab towards M1R was closely resembled that of previously reported mouse antibodies M12B9 (PDB: 4U6H)[34] and 7D11 (PDB: 2I9L)[26] binding to VACV L1R, whereas A129 represents a novel binding epitope (Fig. 3A). Upon superposition, only a minor clash was found between A138 and A129 Fab, which was consistent with their limited competitive binding characteristics (Fig. S3). Similar to the structure of VACV L1R, M1R within the M1R-Fab complex took the conformation of a bundle of α-helices packed against a pair of two-stranded β-sheets (Figs. 3 and S6). Notably, a slight structural variance between MPXV M1R and VACV L1R was observed in the β1 and β3 strands (Fig. S6). In the M1R structure, these strands are discontinuous and segmented into two shorter β strands, which we named β1, β1', β3, and β3', respectively. By contrast, the corresponding region of VACV L1R displayed continuous β1 and β3 strands (Fig. S6). While we observed this structural difference, we could not conclude that the slight difference between MPXV M1R and VACV L1R was a result of their inherent nature, crystal packing effects or antibody interactions.

A138 Fab utilized its three CDRs of the heavy chain and CDR3 of light chain to bind to the loop region connecting the α helices and β sheets of M1R (540 Å² for the heavy chain and 258 Å² for the light chain), which is located on the opposite side of the amino and carboxyl termini of M1R (Fig. 3C). Within the loop region of M1R (A30-E37), interactions occurred with CDR3 residues (T91-F94, L96) of the A138 light chain, as well as with CDR1 (Y33), CDR2 (S52-S54, T56-T57), and CDR3 (Y105) residues of the heavy chain. Additional scattered interaction residues, including N55, K127, and I128 predominantly engaged with residues from CDR1 (R30, D31) and CDR2 (R53, S54, and T57) from the heavy chain of A138 (Figs. 3D, 4B and Table S3). These interactions included 14 hydrogen bonds and two salt bridges (Fig. 4B and Table S3). Notably, the sequence of the A138 heavy chain originates from human germline IGHV3-11, whereas both 7D11 and M12B9 stem from the mouse germline IGHV1S26, which is the closest match to human germline IGHV1-8*02. Additionally, all these antibodies, including A138, 7D11, and M12B9, displayed robust neutralizing activity against VACV. These findings suggested that although these antibodies are from diverse germlines, they could also bind to a shared epitope, reinforcing the notion that this epitope represents a conserved vulnerable site among Orthopoxviruses.

The analysis of the complex structure of M1R-A129 Fab revealed that A129 mainly binds to the β sheets of M1R, specifically the parallel β1-β1' and β3 strands, as well as the connecting loop between α4 and β3 (Figs. 3B and 3D). The heavy chain of A129 Fab comprises the majority of the recognition sites for M1R (Fig. 4A and Table S3). The interface between the heavy chain and M1R buries a total surface area of 431 Å², whereas the area between the light chain and M1R spans only 192 Å² (Fig. 3B). The β1 and β1' strands of M1R (residues N40-N46) interact with CDR2 (W52, N57, T58, and D59), CDR3 (N104-F108) of the A129 heavy chain, as well as CDR3 (A91 and N92) of the A129 light chain. In addition, several sporadic residues on or near the β3 strand also participate in interactions with the heavy chain CDR2 (E62 and D59) and light chain CDR3 (N92, S93, and F94) (Figs. 3D and 4A). These
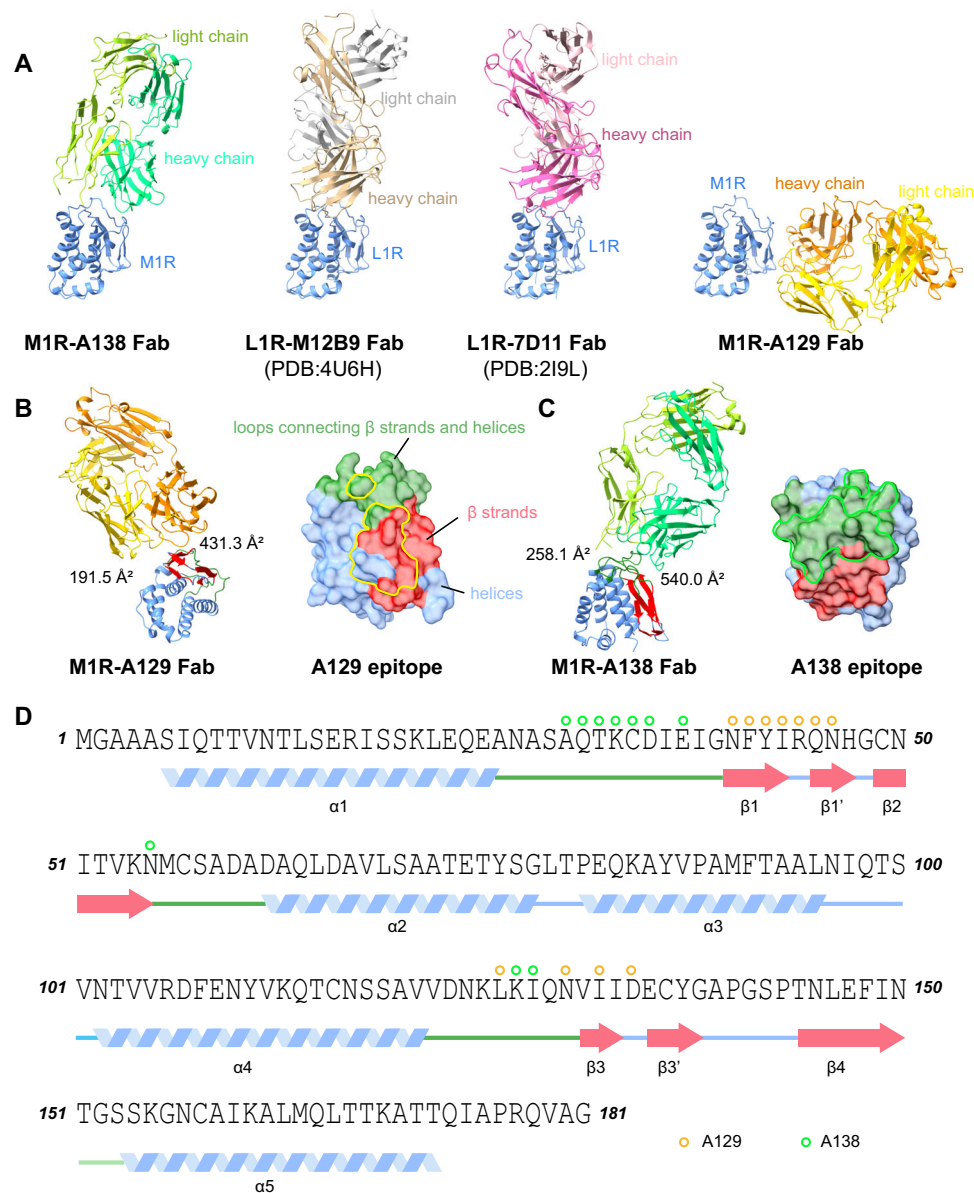
Fig. 3 | Complex structures of A138 Fab and A129 Fab bound to M1R. A Overall structure of antibodies in complex with M1R. MPXV M1R or VACV L1R is colored in cornflower blue; Fab of A138, M12B9, 7D11 and A129 is shown in green, brown, pink and golden, respectively. The heavy chain is shown in a darker color, and all the complex structures are positioned with M1R/L1R in the same orientation. **B** A129 mainly uses its heavy chain to bind the β-sheet of M1R. The buried surface area (BSA) between the A129 heavy chain and M1R is 431 Å² while that of the light chain is 192 Å². The β-sheet of M1R is shown in red and the loops connecting β-strands with helices are shown in green. The epitope of A129 on M1R is labeled by a golden line. **C** A138 mainly uses its heavy chain to bind to the loops connecting β-strands and helices of M1R. The buried surface area (BSA) between A129 heavy chain and M1R is 540 Å² while that of the light chain is 258 Å². The β-sheet of M1R is shown in red and the loops connecting β-strands with helices are shown in green. The epitope of A129 on M1R is labeled by a green line. **D** Sequence and secondary structures of M1R. Contacting residues in M1R for A129 and A138 are indicated by golden and green dots, respectively.

interactions include a total of 11 hydrogen bonds, with six involving the heavy chain and two involving the light chain (Fig. 4A and Table S3).

Analysis of epitopes recognized by B026 and B019 antibodies targeting B6R

We first attempted to solve crystal structures in order to decipher the binding epitopes of neutralizing antibodies targeting B6R. Unfortunately, no crystals appeared for either the B6R-B019 or B6R-B026 Fab complexes. As an alternative, we employed biochemical studies to determine the potential epitopes of these antibodies on B6R. Employing AlphaFold2, we predicted the three-dimensional structure of B6R, revealing that its extracellular domain to consists of a flexible

N-terminal region (residue 1-19), followed by four sushi domains (residues 20 to 239), followed by a stalk region (residues 240-279). The latter is composed of a connecting loop and a partial alpha helix juxtaposed to transmembrane domain (Fig. 5A). Based on the predicted domain, we designed a series of constructs with a 6×His-tag at the C-terminus (Fig. 5B). Utilizing the BLI assay, we assessed the binding affinity of these truncated B6R proteins for B026 and B019. The results indicated that B026 bound to the entire extracellular domain of B6R (residues 19-279; clone 1). By contrast, B026 failed to bind to truncated B6R variants containing only domains 1-4 (clone 2), indicating that the stalk region of B6R (residues 240-279) is indispensable for B026 binding. To validate this specific interaction, we subsequently

Table 1 | Data collection and refinement statistics (molecular replacement)

	M1R-A129 Fab complex	M1R-A138 Fab complex
Data collection		
Space group	P2₁2₁2₁	P2₁
Cell dimensions		
a, b, c (Å)	74.7, 89.3, 100.7	82.4, 136.7, 123.8
α, β, γ (°)	90.0, 90.0, 90.0	90.0, 96.5, 90.0
Resolution (Å)	50.37-2.17 (2.25-2.17)	50.00-3.49 (3.62-3.49)
Rsym or Rmerge	0.117 (1.267)	0.253 (0.779)
I / σI	15.9 (2.0)	5.4 (1.6)
Completeness (%)	99.91 (99.97)	97.31 (87.41)
Redundancy	12.7 (11.6)	5.2 (4.6)
Refinement		
Resolution (Å)	38.33-2.17 (2.25-2.17)	46.67-3.49 (3.62-3.49)
No. reflections	36315 (3566)	33838 (3041)
Rwork / Rfree	0.231/0.251	0.236/0.282
No. atoms		
Protein	4566	17614
Ligand/ion	167	0
B-factor		
Protein	50	73
Ligand/ion	47	
RMSD		
Bond lengths (Å)	0.015	0.007
Bond angles (°)	1.88	1.26
Ramachandran Plot		
Favored (%)	97.32	96.14
Allowed (%)	2.68	3.77
Outliers (%)	0	0.09

Values in parentheses are for the highest-resolution shell

generated constructs with or without the stalk region. B026 exhibited robust binding activity with the constructs containing the stalk region (clones 7, 9, 11 and 12), while showing no binding with fragments lacking this region (clones 3, 4, 5, 6, 8 and 10). The results further confirmed the critical role of the stalk region in mediating B026-B6R interactions (Fig. 5C). In addition, strong binding reactivity was observed between B019 and all truncated B6R proteins containing domain 4 (clones 1, 2, 6, 7, 8, 9, 10 and 11), whereas minimal or no binding occurred with constructs lacking this domain (clones 3, 4, 5 and 12), which suggests the specific recognition of domain 4 by B019 (Fig. 5D).

Prophylactic and therapeutic efficacy of B026 and A138 in mouse models of VACV and MPXV infection

Given the remarkable neutralizing capabilities of B026 and A138, we first evaluated their prophylactic and therapeutic efficacy of VACV infection in a mouse model. Intranasal administration of VACV resulted in significant weight loss and mortality in C57BL/6 mice. Subsequently, mice were administered either B026, A138, or a combination of both either one day before (prophylactic group) or one day after (therapeutic group) VACV challenge (Figs. 6A and S7A). Over the course of 15 days, the animals were closely monitored for changes of body weight and survival.

In the prophylactic group, we initially conducted experiments using a dose of 10^7 plaque-forming units (PFU). The results demonstrated that either a single dose of B026 or the combination of B026 and A138 conferred complete protection (Fig. S7B). To further evaluate

the protective efficacy of the antibodies, we increased the challenge dose to 10^9 PFU. Under this heightened challenge scenario, control mice administrated PBS experienced severe illness, with all animals succumbing by day 10 post-inoculation (p.i.), while a single dose of either B026 or A138 only conferred partial protection (Fig. 6B, C). Specifically, all mice in the A138 and B026 treated groups experienced significant weight loss, with 83% and 66% survival rates, respectively. By contrast, mice pre-treated with the combination of B026 and A138 displayed only slight weight loss during the initial 10 days after viral challenge, followed by subsequent body weight recovery. Meanwhile, those in the control group continued to lose weight without any signs of improvement (Fig. 6B, C). The viral load in the lungs and spleen was assessed via the PRNT assay at four days post-infection (dpi). In the combination treatment group, infectious viral levels were extremely low or undetectable in both the lungs and spleen, even after challenge with 10^9 PFU (Fig. 6F).

Mice mock-treated with PBS in the treatment group showed similar outcomes to those in the prophylactic group, with all succumbing by day 10 p.i. (Fig. 6D, E). Treatment with either B026 or A138 alone resulted in considerable reductions of body weight, with survival rates of approximately 66% and 50% in the A138 and B026 treated groups, respectively (Fig. 6D, E). The levels of infectious virions in the lungs and spleen of these two groups ranged from 10^2 to 10^3 PFU/g, which was lower than in the control group (Fig. 6G). By contrast, animals treated with the combination of B026 and A138 maintained relatively stable body weights and were fully protected from VACV infection (Fig. 6D, E). No virions were detected in the two organs of mice treated with the combination of B026 and A138, whereas the PBS mock-treated mice exhibited viral levels ranging from 10^4 to 10^5 PFU/g (Fig. 6G). Collectively, these results underscored the superior protective efficacy of the combination of B026 and A138 against authentic VACV infection in vivo, using either prophylactic or therapeutic interventions.

To further investigate the protective and therapeutic efficacy of the identified antibodies in a mouse model of MPXV infection, we conducted animal studies using live clade IIb MPXV (MPXV-B.1-China-C-Tan-CQ01)[35] in BALB/c mice[36]. Since the MPXV strain we used does not cause lethality in BALB/c mice, here we measured viral loads in various organs to assess antibody efficacy through qPCR analysis. The results revealed that viral loads were highest in the lungs (3.17×10^5 copies/mL, PBS group), while being lower in the liver and spleen (Fig. 7A, B). In both prophylactic and therapeutic groups, antibody-treated mice exhibited reduced viral loads in the lungs, liver, and spleen compared to the control group (PBS group) (Fig. 7A, B). This demonstrating that the antibodies used in our study effectively provided protection against MPXV infection. Notably, co-administration of the A138 and B026 antibodies resulted in significantly lower viral titers in all organs, suggesting that the combination of two antibodies targeting different antigens enhanced protective efficacy. However, the bispecific antibody ScFvA138B026 containing both A138 and B026 binding regions exhibited a similar, or slightly reduced, protective effect compared to A138 or B026 alone.

Discussion

In this research, we utilized the phage display technique to isolate a diverse and substantial array of human antibodies targeting the M1R and B6R proteins of MPXV. Detailed neutralizing assays indicated that optimal protection could be achieved by combining two highly potent neutralizing antibodies, each targeting a different antigen—M1R on the surface of MV and B6R on the surface of EV. Protection was effective when using a combination of B026 and A138, which agreed with findings in other Orthopoxviruses. In addition, we characterized the specific binding epitopes of these four antibodies targeting M1R and B6R via crystallographic studies and biochemical analysis. Our findings
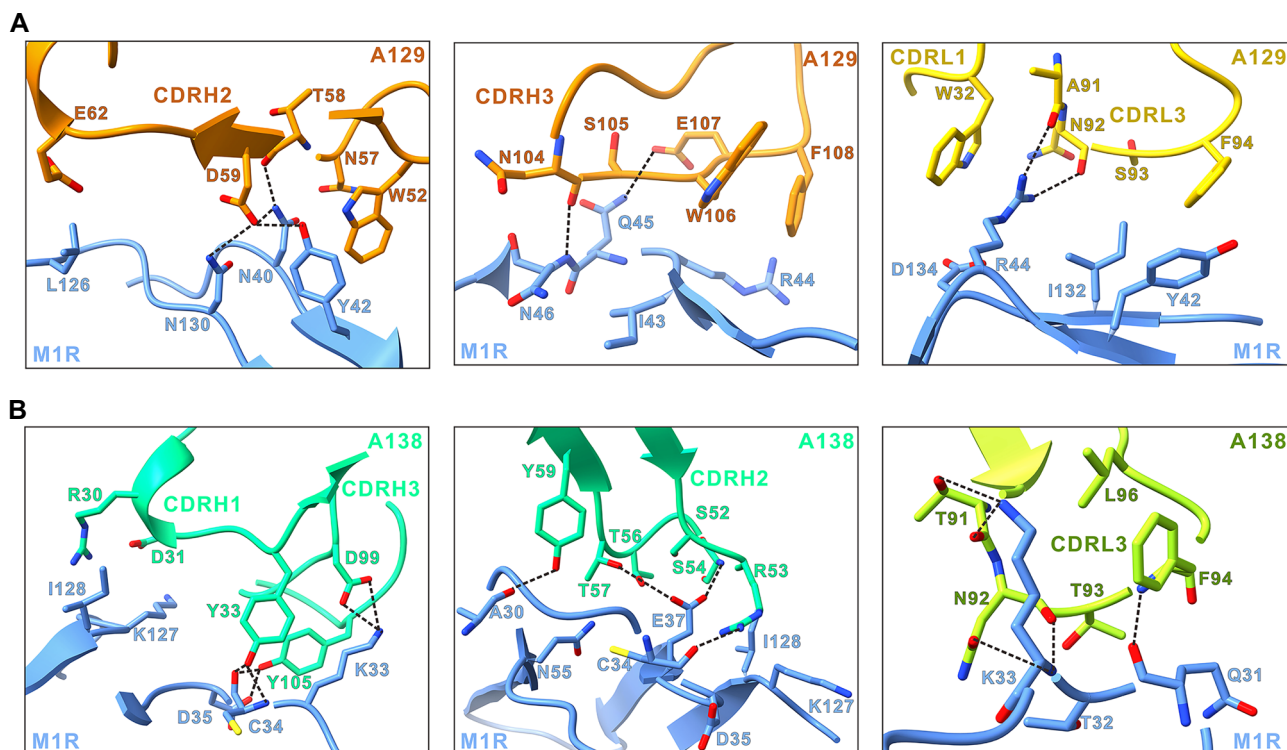
Fig. 4 | The binding interface between M1R and A129/A138 Fab. Detailed interactions of the A129 Fab (**A**) and A138 Fab (**B**) with M1R. Hydrogen bonds and salt bridges are indicated by dashed lines. M1R is shown in cornflower blue. The heavy and light chains of A129 are shown in dark goldenrod and yellow, respectively. The heavy and light chains of A138 are shown in spring green and green yellow, respectively.

provide valuable insights and potential guidance for future MPXV therapy, highlighting the efficacy of employing two potent and broadly neutralizing antibodies targeting M1R or B6R.

In this study, we utilized a fully human antibody library, comprising samples derived from PBMC of over 2000 healthy donors aged between 20 and 60 years old for antibody screening. Notably, mandatory vaccination with the vaccinia virus Tiantan strain (VACV-VTT) for the general population ceased in 1980. Therefore, donors aged over 45 might have received historical vaccination with the VACV-VTT, leading to cross-reactivity against MPXV surface proteins, which may have provided neutralizing protection against VACV-VTT even after more than 40 years[37]. Additionally, individuals born after 1980 may also exhibit a serum antibody response against MPXV surface proteins due to their exposure to some self-limiting Orthopoxviruses, as previously observed by Xia et al.[37]. Thus, the human antibody library utilized in our study potentially contains a diverse array of potent and distinct neutralizing antibodies against MPXV antigens, confirming the success of neutralizing antibody screening.

The correlation between epitopes and the neutralizing capacities of M1R and B6R antibodies offers valuable insights for the identification of vulnerable and functional sites. Among M1R antibodies, our structural studies delineated two distinct functional epitopes on M1R. One epitope, targeted by A138 and 7D11, is situated away from the C-terminal region, connecting the transmembrane domain on the surface of MV. This epitope is theoretically the most vulnerable, as it remains accessible regardless of the rotation of M1R around its stalk. By contrast, the epitope targeted by A129 is located at the side of M1R, which becomes less accessible when M1R rotates towards this region. The buried surface area and neutralizing activity of A129 was significantly lower than that of A138, likely due to reduced accessibility. As for B6R antibodies, four distinct binding epitopes are roughly clustered based on competitive BLI assays. After further neutralization experiments and biochemical analyzes, we found that two highly

potent neutralizing antibodies (B026 and B019) target domain 4 or close to the stalk region. This was consistent with a previous study on B5R, with neutralizing antibodies binding around domain 4 or the stalk region[38]. The binding of these antibodies to B6R likely modulates its flexibility on the virion surface, affecting its interaction with binding partners. In this study, antibodies sharing a similar epitope with B019 often exhibited low neutralization activity, indicating that this epitope might represent a weak neutralization target.

M1R, a myristoylated antigen located on the surface of the MV form of MPXV, was predicted to be a crucial component of the entry fusion complex (EFC). Its homolog, L1R, has been reported to play roles in morphogenesis, the formation of infectious virions, and virus entry[39,40]. Additionally, the discontinuous loops 1, 2, and 3, targeted by A138 and several other highly potent neutralizing antibodies, have been identified as interaction domains for non-glycosaminoglycan (GAG) receptors[41]. As a result, antibodies such as A138 are predicted to exert their neutralizing effects by hindering the binding of M1R to non-GAG molecule(s) receptor, potentially impeding virus entry[41,42]. As a surface protein on EV, B6R is known to be associated with the regulation of complement activation[42]. The neutralization mechanisms of B6R antibodies are complex, involving the recruitment of complement C1q, the covalent attachment of C3 to the virion surface hindering binding to target cells, as well as the induction of antibody-dependent cell-mediated cytotoxicity[43]. Although we established the potent protective effects and detailed epitopes of M1R and B6R antibodies, a clear explanation of their neutralization mechanisms remain elusive. Future studies on the function of Orthopoxvirus proteins might provide a better understanding of the underlying processes.

There are two limitations in our studies. First, in the neutralization assay, we assessed the in vitro neutralizing activity of combined antibodies using a mixture of MV and EV forms of MPXV/VACV. However, the EV forms are fragile and easily converted into MV. To evaluating the protection effect of antibodies targeting the EV form, excess MV
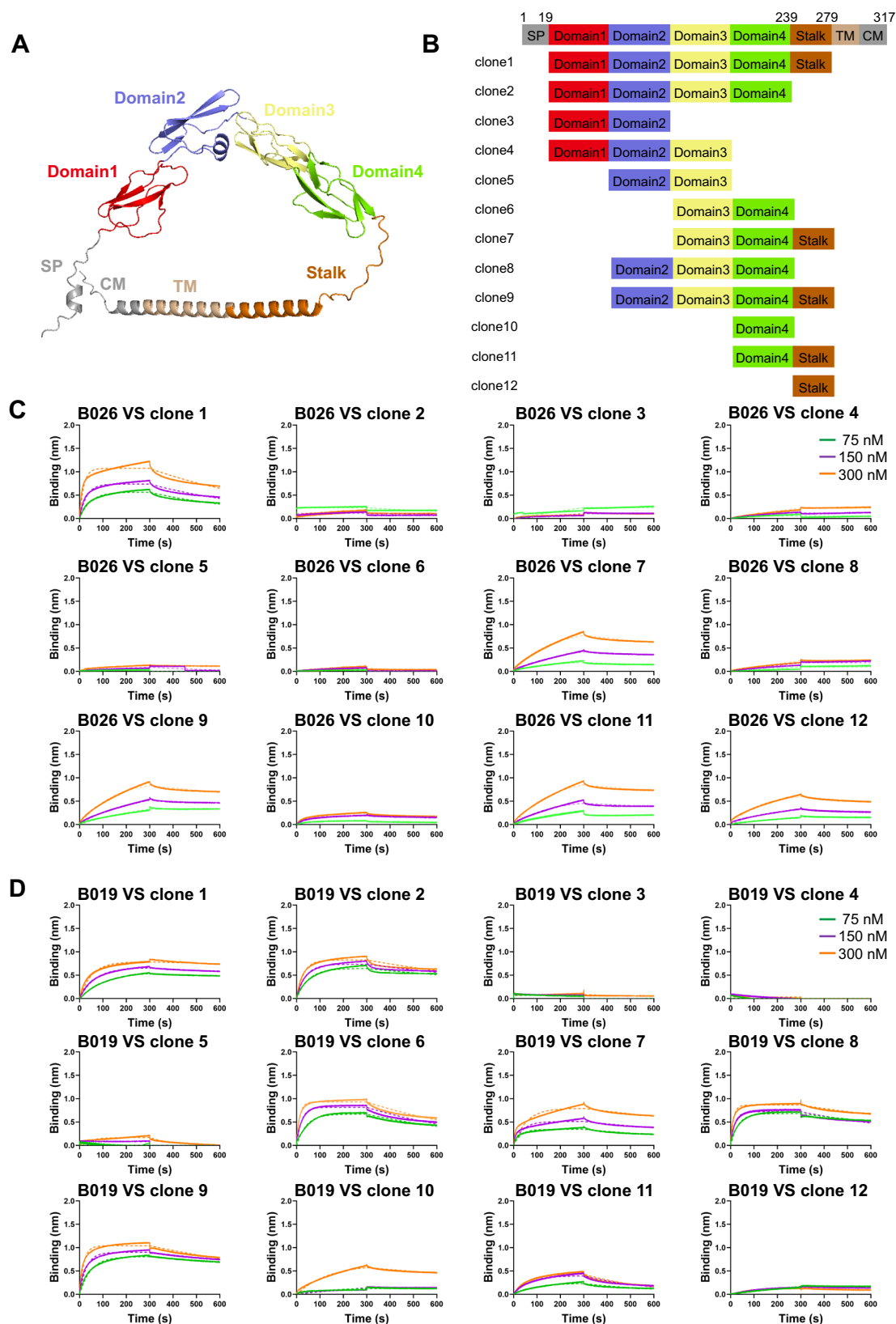
Fig. 5 | Epitopes analysis of B026 and B019. A Modeled structure of the B6R protein predicted using AlphaFold2. The four domains of B6R are shown in red (domain 1), blue (domain 2), yellow (domain 3), and green (domain 4). The stalk region is shown in brown. B Schematic diagrams representing the structures of a series of truncated B6R proteins variants. All these truncated B6R constructs contain a 6×His tag at the C-terminus, which was used for protein purification. C, D Binding of B026 (C) and B019 (D) to different fragments of B6R. Different fragments of B6R were loaded onto the surface of biosensors, and individual antibodies were tested at three concentrations (75 nM, 150 nM, 300 nM). The association and dissociation curves are shown. The dashed lines represent the fitted curves based on the experimental data. Source data are provided as a Source Data file.
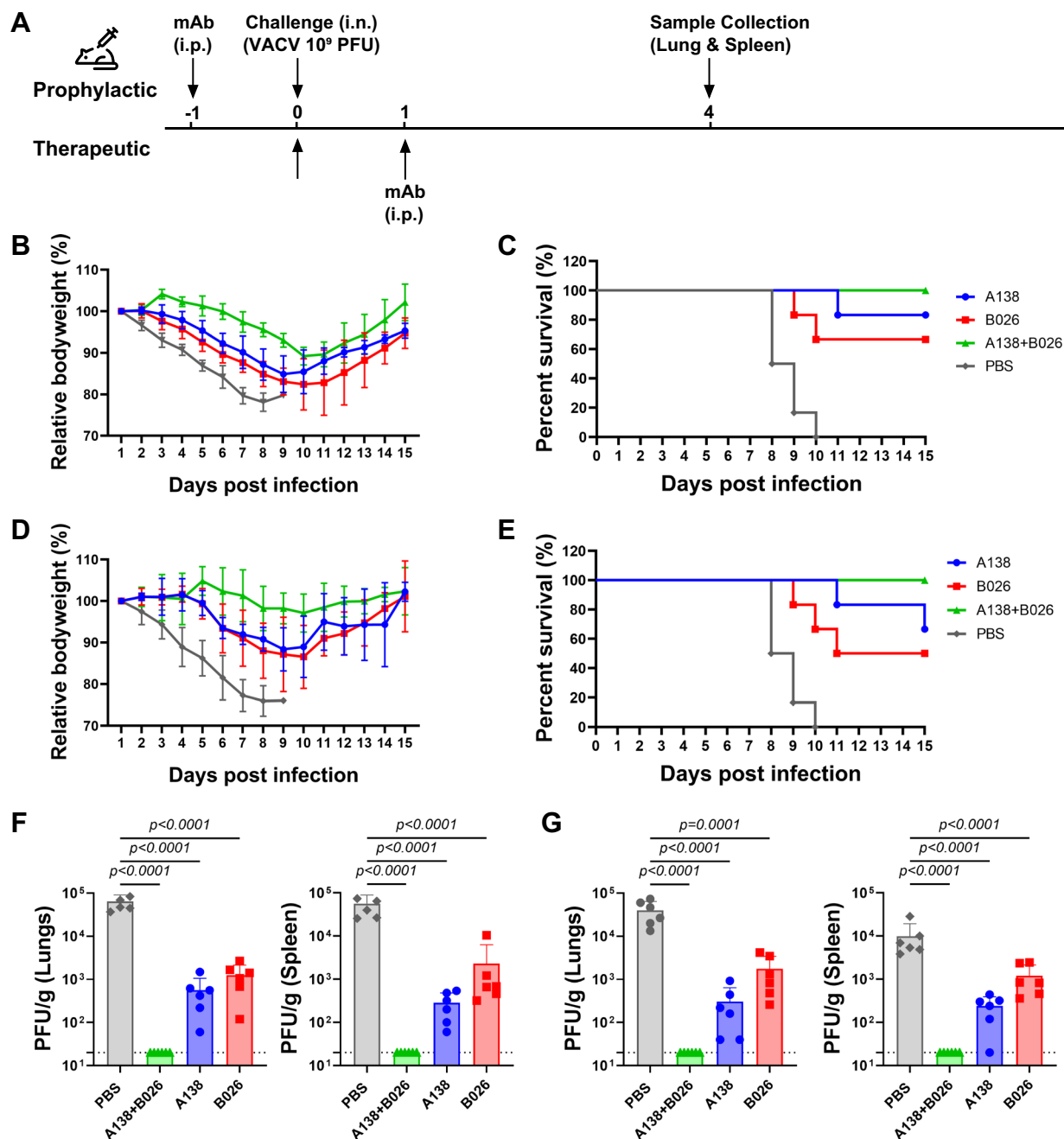
Fig. 6 | Prophylactic and therapeutic efficacy of B026 and A138 in a high-dose VACV-challenge mouse model. A Schematic diagram of the prophylactic and therapeutic models. C57BL/6 mice were randomly divided into 4 groups (*n* = 6 per group). For the prophylactic model, mice were injected intraperitoneally (i.p.) with PBS, individual antibodies (A138 or B026) or antibody cocktail (A138 and B026) at 24 hrs before challenged with a high-dose (10^9 PFU) of VACV. For the therapeutic model, mice were injected i.p. 24 hrs after challenge with 10^9 PFU VACV. Body weight (**B**, **D**) and survival curves (**C**, **E**) were recorded. **B**, **C** show data for prophylactic model while (**D**) and (**E**) for the therapeutic model. **F**, **G** Viral titers in the lungs and spleen of mice in the prophylactic (**F**) and therapeutic groups (**G**). The data represent means ± SEM, indicated by error bars. The significance of differences between groups was assessed using one-way ANOVAs followed by Dunnett's multiple comparisons test for multiple comparisons. Source data are provided as a Source Data file.

antibody 7D11 was added to deplete the residual MV[38]. However, we didn't involve 7D11 into the MV + EV neutralization assay, as 7D11 would interfere the neutralization effect of anti-M1R antibodies. Although we tried to mix the MV and EV form in equal molar ratio, there are actually more MV forms in the mixture. This higher MV/EV ratio may affect the accuracy of antibody neutralizing activity assessment, although it does not alter the final conclusion.

The second limitation we need to point out is that we used a BALB/c mice model infected with MPXV (MPXV-B.1-China-C-Tan-

CQ01)[35], which belongs to lineage B.1, clade IIb. We chose this model based on a previous study using WIBP-MPXV-001, also from lineage B.1, clade IIb[36,44]. In WIBP-MPXV-001 infected BALB/c model, moderate viral loads and significant histopathological changes were observed in the lungs, with minimal effects on the body weight and overall health. This model has been successfully employed to evaluate the immunoprotective efficacy of a monkeypox vaccine. In our current model, viral DNA was detected in lung, liver and spleen, with lungs as the major site. The viral load in the lungs of PBS group was
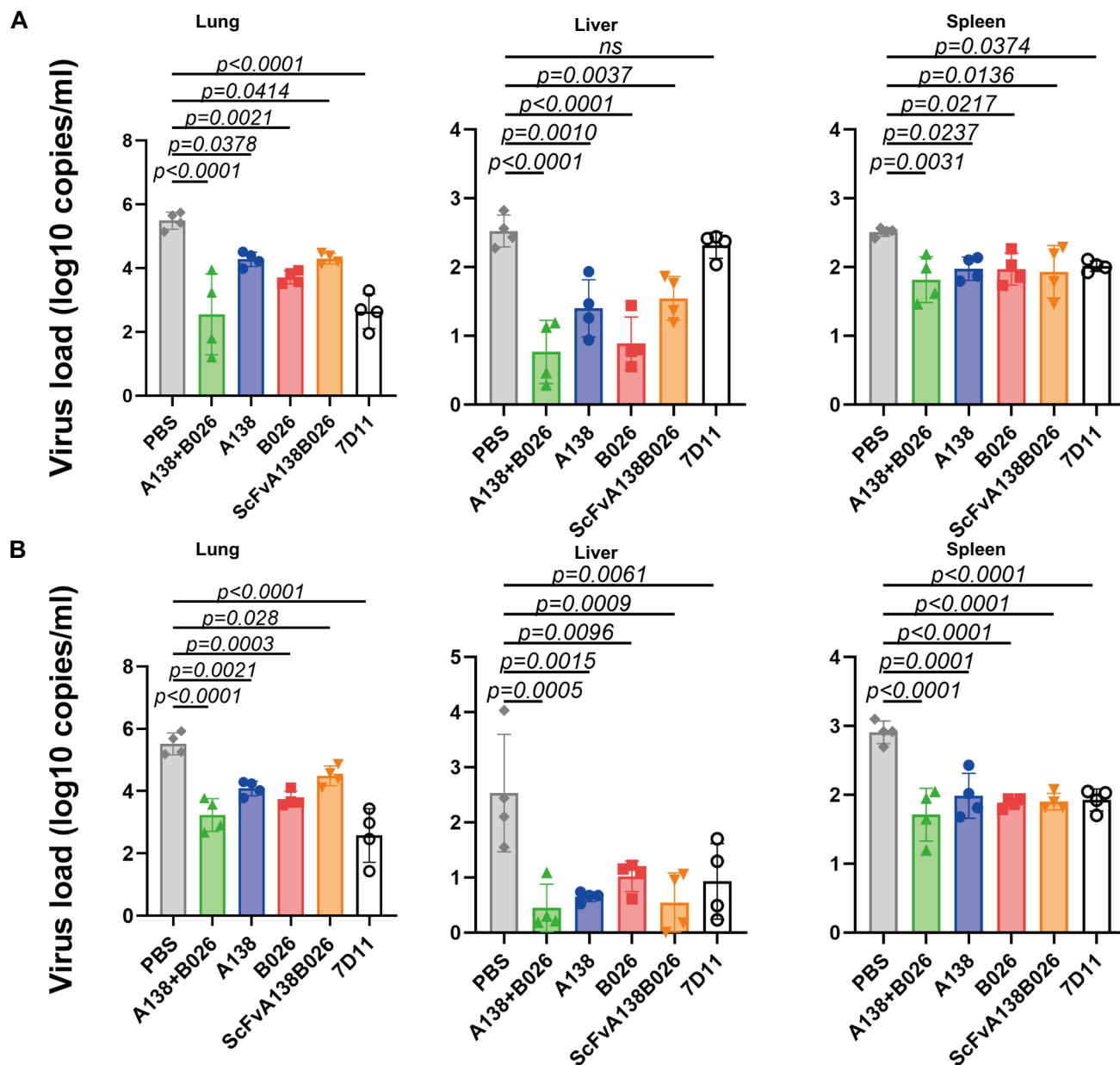
Fig. 7 | Prophylactic and therapeutic efficacy of B026 and A138 in a MPXV-challenged mouse model. A Viral titers in the lungs, liver and spleen of mice in the prophylactic model. **B** Viral titers in the lungs, liver and spleen of mice in the therapeutic model. BALB/C mice were randomly divided into 6 groups (with $n = 4$). For the prophylactic model, mice were injected intraperitoneally (i.p.) with PBS, individual antibodies (A138, B026, ScFvA138B026, or 7D11) or antibody cocktail (A138 and B026) at 24 hrs before challenged with 10^6 PFU of MPXV. For the therapeutic model, mice were injected i.p. 24 hrs after challenged with 10^6 PFU of MPXV. The data represent means ± SEM, indicated by error bars. The significance of differences between groups was assessed using one-way ANOVAs followed by Dunnett's multiple comparisons test for multiple comparisons. Source data are provided as a Source Data file.

3.17×10^5 copies/mL. The mice exhibited only mild weight loss and slight lethargy, without severe disease phenotypes such as hunched posture, significant weight loss, or mortality. While this model is not perfect, it is the only MPXV model we could access at the moment. Based on this model, we used qPCR to assess viral loads of different groups, including A138, B026, A138 + B026, ScFvA138B026. Generally speaking, the combined A138 and B026 displayed the most potent protection in both preventive and therapeutic groups. Surprisingly, ScFvA138B026 exhibited suboptimal protective and therapeutic effects compared to the single antibodies, possibly due to variations in its distribution, metabolism, and clearance in vivo. We also included the control antibody 7D11, targeting L1R protein of VACV, which has shown strong neutralizing activity[29]. The protective

and therapeutic effects of 7D11 were found to be comparable to, or even slightly better than, those of the combined A138 and B026. This suggests that the combination of antibodies may not be necessary for in vivo protection against MPXV and could potentially be substituted with a single potent anti-MV antibody, such as 7D11. This observation is consistent with findings in other literature[22]. However, we could not exclude the possibility that observed discrepancies might arise from the specific mice model and experiment system we used. Our examination of viral load via qPCR cannot distinguish infectious virions from residual virus. Future studies should incorporate plaque assays and more focus on developing robust mice models to accurately assess the efficacy of monoclonal antibodies.

Methods

Ethics statement

The research is performed under the study protocol AMMS-11-2023-015. All animal studies were performed in strict accordance with the guidelines set by the Chinese Regulations of Laboratory Animals and Laboratory Animal-Requirements of Environment and Housing Facilities. Mice (C57BL/6 and BALB/c) were housed in standard ventilated cages (3–5 mice per cage) under specific pathogen-free (SPF) conditions. The animal room was maintained at a 12-h light/dark cycle (lights on at 7:00 AM), ambient temperature of $22 \pm 2\,°C$, and relative humidity of $50 \pm 10\%$. Food and water were provided ad libitum, and bedding was replaced twice weekly. All animal procedures were reviewed and approved by the Animal Experiment Committee of Laboratory Animal Center, AMMS, China.

Cells and viruses

African green monkey kidney Vero (ATCC, #CCL-81) was maintained in DMEM medium (Gibco, 11965118) supplemented with 10% fetal bovine serum (FBS, Gibco, 10091148), penicillin (100 U/mL) and streptomycin (100 μg/mL) (Gibco, 15070-063). Vaccinia virus TianTan strain (VACV-VTT), preserved and amplified in our laboratory, was propagated and titered in monolayer cultures of Vero cells. Replication-deficient MPXV virus (MPXV G9R + A1L-KO)[27], preserved and amplified in our laboratory, was propagated and titered on Vero cells expressing G9R and A1L proteins of MPXV (VERO E6 G9R + A1L Cell, maintained and expanded in our laboratory). MPXV (MPXV-B.1-China-C-Tan-CQ01)[35] living virus was propagated and titered by Changchun Veterinary Research Institute, Chinese Academy of Agriculture Sciences. VACV and replication-deficient MPXV were manipulated under BSL-2 conditions. MPXV were manipulated under BSL-3 conditions.

Viruses preparations for neutralization assay

MV and EV were prepared as previously described[45]. For EV stock preparation, Vero or VERO E6 G9R + A1L Cell were infected at a multiplicity of 0.5 PFU/cell. When cytopathic effect was complete (4 days for replication-deficient MPXV and 48 h for VACV) the culture supernatant was harvested and cleared by centrifugation (30 min at $2000 \times g$), stored at 4 °C, and used within 2 weeks of preparation. The titers of the stock were determined in the presence of an MV-neutralizing anti-L1R MAb (7D11) to neutralize any contaminating MV or damaged EV[38]. For MV stock preparation[23,46], Vero or VERO E6 G9R + A1L Cell were infected at a multiplicity of 0.5 PFU/cell. Cells were harvested at 5 days (for replication-deficient MPXV) or 48 h (for VACV). Virus was isolated by rapidly freeze-thawing the cell pellet three times in DMEM supplemented with 1% heat-inactivated FCS. Cell debris was removed by centrifugation at $700 \times g$ for 8 minutes. The virus was sonicated for 40 seconds, then layered over 36% sucrose. The virus was pelleted by centrifugation at 13,500 rpm ($33,000 \times g$) for 80 minutes at 4 °C. The pellet was resuspended in DMEM with 1% heat-inactivated FCS. The virus solution was aliquoted into 1.5 mL Eppendorf tubes (50 μL per aliquot) and stored at −80 °C for long-term preservation.

For the preparation of the mixtures of MV and EV forms of VACV and replication-deficient MPXV, we diluted the EV and MV viruses with serum-free DMEM medium to 400 pfu/100 μL. Then, the two diluted viruses were mixed in equal volumes to obtain mixtures of MV and EV. The residual MV fraction in the EV stocks resulting in a higher proportion of MV in the mixture. The mixture was freshly prepared each time it was used.

Viruses preparations for in vivo prophylactic and therapeutic study

For VACV preparation[47], Vero cells are infected at a multiplicity of infection (MOI) of 0.1 PFU/cell. Incubate the infected cells at 37 °C for 2 h to allow for virus attachment and entry. After this period, replace the medium with fresh DMEM containing 2% FBS to support cell growth. Continue incubation at 37 °C for 48–72 h until a complete cytopathic effect (CPE) is observed. To harvest the VACV, freeze-thaw the infected cell cultures three times at -80 °C. After the final thaw, briefly centrifuge the samples at 4 °C to pellet the cells, and discard the cell debris. Filter the supernatant through a 0.45 μm filter to remove any remaining cellular debris. Transfer the filtered virus solution to ultracentrifuge tubes containing a 36% sucrose cushion, and balance the tubes before centrifuging. Centrifuge at $32,900 \times g$ for 80 minutes at 4 °C. After centrifugation, carefully discard the supernatant and resuspend the viral pellet in an appropriate volume of PBS. Aliquot the virus solution into clean 1.5 mL Eppendorf tubes (50 μL per aliquot), and store the aliquots at -80 °C for long-term preservation.

MPXV (MPXV-B.1-China-C-Tan-CQ01) living virus was propagated and titered by Changchun Veterinary Research Institute, Chinese Academy of Agriculture Sciences. Vero cells were infected with MPXV at a multiplicity of infection (MOI) of 0.1 PFU/cell and incubated at 37 °C for 4–5 days, until a complete cytopathic effect (CPE) was observed. To harvest the virus, infected cells were subjected to the freeze-thaw cycles at -80 °C. After the final thaw, samples were briefly centrifuged at 4 °C to pellet the cells, and the resulting cell debris was discarded. The supernatant was then filtered through a 0.45 μm filter to remove any remaining cellular debris. The virus solution was aliquoted into clean 1.5 mL Eppendorf tubes (50 μL per aliquot) and stored at -80 °C for long-term preservation.

Protein expression and purification

The recombinant MPXV proteins M1R and B6R used for screening were produced using Expi293F system whereas those used for crystallization were expressed in insect cell system. The proteins produced in insect cell system harbored a less potential glycosylation, which was in favor for crystallization.

For screening, the extracellular domain of M1R (residue 1-181) and B6R (residue 20-279) were constructed on the mammalian expression vector pCAGGS with IL-2 signal peptide and a C-terminal 6×His Tag. The expression vectors were transiently transfected into 293F cells (ATCC, CBP60437) by polyethylenimine (PEI) (Kairuibiotech, K20001). Protein was purified from filtered cell supernatants using Ni-NTA resin (Solarbio, P2010) before undergoing additional purification by size-exclusion chromatography in 20 mM Tris, 200 mM NaCl, pH 8.0.

For crystallization, the extracellular domain of M1R (residue 1-181) was cloned into the pFastBac dual vector with a gp67 signal peptide and a C-terminal 6×His tag for purification. The construct was transformed into DH10Bac component cells, and the extracted bacmid was then transfected into Sf9 cells using Cellfectin II Reagent (Invitrogen). The low-titered viruses were harvested and then amplified to generate a high-titer virus stock, which was used to infect Hi5 cells at a density of 2×10^6 cells/mL. The supernatant of cell culture containing the secreted M1R was harvested 60 h after infection, concentrated and buffer-exchanged to HBS (10 mM HEPES, pH 7.2, 150 mM NaCl). M1R was captured by Ni-NTA resin (GE Healthcare) and eluted with 300 mM imidazole in HBS buffer. M1R was further purified by gel filtration chromatography using the Superdex 200 column (GE Healthcare) pre-equilibrated with HBS buffer. Fractions containing M1R were collected and frozen at -80 °C.

Screening of M1R and B6R antibodies

Candidate antibodies were screened from a phage-display fully human antibody library (simplified as ST-ST-HuNAL, constructed by Sanyou Bio with the capacity of 2.2×10^{11}, Fab format) (https://www.sanyoubio.com.cn) by solid-phase immunotube screening method against recombinant M1R and B6R proteins of MPXV as targets. Briefly, M1R or B6R protein in carbonate buffer was coated on Nunc™ Immuno Max-iSorbTubes (Thermo Fisher Scientific, 472230), overnight at 4 °C. The next day, washing with PBS 3 times, then blocking buffer, 3% (w/v) bovine serum albumin (BSA), was added to the tube and incubated at

room temperature for 2 h. Washing with PBS 3 times, added the phage library solution and incubated for 1 h at room temperature. After washing with PBS with 0.1% Tween-20 (PBST) 20 times to remove the non-specific phage. Bound phages were eluted by 30 min of digestion using 500 µL of 0.25 mg/mL trypsin at room temperature with rotation. The reaction was stopped with 10 µL 10% AEBSF. The eluted phages were used to infect E. coli XL1-blue for titer determination. The amount of input phage of the next rounds was 1×10^{12} PFU, and the washing time was 20 times. The output phage titer of every round of panning was measured.

Phage ELISA

Over 500 phage clones were randomly selected during the final round of panning, and their antigen-binding ability was analyzed by ELISA. A 96-well plate was coated with 100 µL of 1 µg/mL antigen at 4 °C overnight. The next day, the plate was washed 3 times with PBS buffer and blocked with 3% BSA buffer at room temperature for 1 h. Washing with PBST 5 times, 25 µL of supernatant containing soluble fragment in 75 µL of PBS supplemented with 3% (w/v) BSA was added to each well of the ELISA plate, and the plate was incubated at room temperature for 1 h with gentle agitation. The wells were washed with 5 times with PBST, and 100 µL of 1:10,000 anti-M13-HRP (SinoBiological, 11973, Monoclonal Mouse IgG1 Clone #MM05) antibody in PBS supplemented with 3% (w/v) BSA was added to each well. The plate was then incubated at room temperature for 1 h with gentle agitation. The wells were washed 5 times with PBST and 1 time with PBS, and 100 µL of TMB (Invitrogen™, 002023) solution was added to each well. The reaction was stopped with 50 µL of ELISA terminating solution (New Cell&Molecular Biotech, E40500), and the absorbance was read at 450/620 nm using an ELISA plate reader.

Construction, Expression, and Purification of M1R and B6R antibodies

The antibody was prepared using Expi293F system. Briefly, after phagemid extraction, the heavy-chain and light-chain was amplified via PCR. The heavy-chain and light-chain gene were cloned into antibody expression vectors encoding the constant regions of human IgG1 by enzymatic assembly[48]. The construct was transferred into 293F cells. Plasmids containing the heavy-chain and light-chain of the antibody were mixed with PEI and added to the prepared cell suspension with gentle shaking. The cell culture was then transferred and incubated at 37 °C in the shaker with 7% CO_2. Five days after transfection, the culture supernatant containing antibody was collected and centrifuged at $12,000 \times g$ for 10 min and the resulting supernatant was subjected to affinity purification with protein G (Solarbio, R8300). Antibody was eluted with 100 mM Glycine-HCl (pH 3.0) and then neutralized with 1 M Tris-HCl. The purity of the eluted proteins was assessed by 12% SDS-PAGE and Western blot. Finally, the purified antibody was exchanged into PBS buffer using a centrifugal filterunit (Millipore, UFC8010). Aliquots were made and stored in −80 °C. The IGBLAST program (https://www.ncbi.nlm.nih.gov/igblast/igblast.cgi) was used to analyze germline genes, germline divergence, the framework region (FR) and the loop length of CDR3 for each antibody clone.

ELISA

ELISA was used to measure the EC_{50} of antibodies. Each antigen (M1R and B6R) was diluted to 1 µg/mL with coating buffer followed by coating the 96-well plates with each antigen, respectively, at 4 °C overnight. The antibodies were serially diluted by 3-fold and placed into the plate coated with 3% (w/v) BSA at 37 °C for 1 h. After washing with PBST, the plate was incubated with HRP-conjugated goat anti-human IgG (Santa Cruz, sc-2453) at 37 °C for 1 h and color reaction was developed by adding 100 µL TMB for 5 min followed by adding 50 µL of ELISA terminating solution to stop the reaction. The absorbance was measured at 450/620 nm using an ELISA plate reader.

Biolayer interferometry (BLI) analysis

Experiments were performed on an Octet RED biosensor instrument (Pall ForteBio; Menlo Park) essentially. FortéBio data analysis software, version 12.1.was used to analysis data from Biolayer interferometry (BLI). Briefly, biosensors were pre-wetted in running buffer containing DPBS, 0.1% BSA, and 0.05% Tween-20. M1R or B6R linked with His-tag were loaded onto Ni-NTA biosensor tips (ForteBio, 18-5101) at a concentration of 5 ug/mL. Biosensors were then incubated with fold dilutions of antibodies. For affinity testing of bsAbs, we used a 1:1 fitting model for curve fitting, as it provided a better fit than the bivalent analyte model. However, the 1:1 model may not fully reflect true monovalent interactions, as binding kinetics could be influenced by multivalent interactions or non-specific binding.

For cross-competition assay, antibody-antigen complexes were tested for the ability to bind a second antibody in sandwich assay. Briefly, biosensors were pre-wetted in running buffer containing DPBS, 0.1% BSA, and 0.05% Tween-20. M1R or B6R linked with His-tag were loaded onto Ni-NTA biosensor tips at a concentration of 5 ug/mL. Biosensors were then incubated with primary antibodies at a concentration of 300 nM. Following this, secondary antibodies were loaded at a concentration of 150 nM. The extent of antibody-antigen association was determined as the wavelength shift in nm and calculated as a percentage after normalization. In this calculation, 0%-20% was considered complete competition, 20%-60% was considered partial competition, and over 60% was considered non-competition. Experiments were performed in duplicate.

Virus neutralization assays

The neutralizing activity of antibodies was determined using MV or EV forms of VACV, or MPXV defective virus in a PRNT assay. Neutralization of VACV EV was performed using 10% guinea pig complement (Solarbio, S4990), and neutralization of VACV MV was performed without complement. For EV neutralization, MV was depleted with blocking mAbs MV-neutralizing anti-L1R MAb (7D11) at 20 µg/mL. The antibodies were serial dilutions (3 or 5-fold) with serum-free DMEM medium with or without complement, and then mixed with an equal volume of virus (200 pfu/100 uL) and incubated at 37 °C for 1 h. The mixture was added to the 6-well cell plates laid with Vero cells or Vero E6 G9R + A1L cells one day prior (1.5×10^5 cells/well) and incubated for 2 h before replacing media with DMEM containing 2% FBS (v/v) and 0.3% (w/v) methylcellulose (Sinopharm, LA1810501). After incubation for 48 h, the cells were fixed with 4% PFA, stained with crystal violet solution for 0.5 h, and rinsed with distilled water[23]. For the EV + MV neutralization assay, 7D11 was not used as it would affect anti-M1R antibodies, while complement was included to assist the efficacy of anti-B6R antibodies.

In vivo prophylactic and therapeutic study

To evaluate the prophylactic and therapeutic effects of antibodies, six- to eight-week-old male C57BL/6 mice (purchased from Charles river, 213) were randomly assigned to four groups. Mice in the A138 and B026 groups received a single intraperitoneal injection of 20 mg/kg of antibody. The A138 + B026 group received a 1:1 combination of the two antibodies, with a total dose of 20 mg/kg. The control group received an equivalent volume of 400 µL PBS. For viral challenge, mice were intranasally inoculated with either 10^7 PFU or 10^9 PFU of VACV-VTT. Mice were monitored daily for signs of morbidity, and euthanasia was performed according to IACUC guidelines when weight loss exceeded 30% of the initial body weight. Virus titers were quantified by homogenizing the lungs and spleens of individual mice, followed by viral plating on confluent Vero cell monolayers.

To further evaluate the prophylactic and therapeutic efficacy of antibodies, we conducted a study using a mouse model infected with

live MPXV[36]. Three- to four-week-old male BALB/c mice (purchased from Charles river, 211) were randomly assigned to six groups: 7D11, A138, B026, A138 + B026, ScFvA138B026, and PBS. Mice in the 7D11, A138, and B026 groups received a single intraperitoneal injection of 20 mg/kg of antibody. The A138 + B026 group received a 1:1 combination of both antibodies at a total dose of 20 mg/kg. The bivalent antibody group received a total dose of 26.34 mg/kg, adjusted to match the molar concentration of the other antibody groups. The control group was injected with 400 μL of PBS. Mice were intranasally inoculated with 10^6 PFU of MPXV. Daily monitoring for signs of morbidity was performed, and euthanasia was carried out in accordance with IACUC guidelines for mice that experienced a weight loss exceeding 30% of their initial body weight. Mice were euthanized four days after challenged with MPXV, and their organs were collected for analysis. Virus titers were assessed by homogenizing the lungs, liver, and spleens of individual mice, followed by quantification of viral copies.

Crystallization and data collection

The M1R (residue 1-181) expressed in insect cell and the Fab fragment of A138 or A129 were mixed at a molar ratio of 1:1.2, incubated for 2 h at 4 °C and further purified by gel-filtration chromatography. The purified complex concentrated to ~10 mg/mL in HBS buffer (10 mM HEPES, pH 7.2, 150 mM NaCl) was used for crystallization. The screening trials were performed at 18 °C using the sitting-drop vapor-diffusion method by mixing 0.15 μL protein with 0.15 μL reservoir solution. Crystals were successfully obtained in 0.2 M Lithium citrate tribasic tetrahydrate, 20% w/v polyethylene glycol 3,350 for M1R-A129 complex and 0.1 M Magnesium formate dihydrate, 15% w/v Polyethylene glycol 3,350 for M1R-A138 complex, respectively. Both diffraction data of M1R-A129 Fab and M1R-A138 Fab complex were collected at 100 K and at a wavelength of 0.97918 Å on the BL18U1 beam line of the Shanghai Synchrotron Research Facility.

Structure determination and refinement

The complex structure of M1R-A129 Fab and M1R-A138 Fab were determined by the molecular replacement method with PHASER (CCP4 Interface 7.1.007)[49]. The search models were the structure vaccinia L1 (PDB:4U6H) and the structures of the variable domain of the heavy and light chains available in the PDB with the highest sequence identities. Subsequent model building and refinement were performed using COOT v.0.9.2 and PHENIX v.1.18.2, respectively. Final Ramachandran statistics: 97.32% favored, 2.68% allowed and 0.00% outliers for the final M1R-A129 Fab complex; 96.14% favored, 3.77% allowed and 0.09% outliers for the final M1R-A138 Fab complex.

Statistical Analysis

Statistical analyzes were conducted using Prism 8.0 (GraphPad). EC_{50} values were determined after log transformation of antibody concentration using sigmoidal dose-response nonlinear fit analysis, and IC_{50} values were determined using dose-response inhibition nonlinear fit model as described previously. Differences among animal groups were evaluated using One-way analysis of variance (ANOVA), followed by Dunnett's multiple comparisons test for multiple comparisons. A significance level of $p < 0.05$ was adopted for all statistical tests. The bars within the graphs represent mean values, and the error bars indicate standard error of the mean (SEM).

Reporting summary

Further information on research design is available in the Nature Portfolio Reporting Summary linked to this article.

Data availability

The crystal structure data generated in this study have been deposited in the Protein Data Bank (PDB) with accession code 8ZU9 for A129/ M1R, and accession code 8ZUA for A138/M1R. All data generated in this study are provided in the Supplementary Information/Source Data file. Source data are provided with this paper. The crystal structure data used in this study are available in the PDB database under accession code 4U6H for M12B9/L1, and accession code 2I9L for 7D11/ L1R. Source data are provided with this paper.

References

1. Khodakevich, L., Jezek, Z. & Messinger, D. Monkeypox virus: ecology and public health significance. *Bull. World Health Organ* **66**, 747–752 (1988).
2. Arita, I., Jezek, Z., Khodakevich, L. & Ruti, K. Human monkeypox: a newly emerged orthopoxvirus zoonosis in the tropical rain forests of Africa. *Am. J. Trop. Med Hyg.* **34**, 781–789 (1985).
3. Lum, F. M. et al. Monkeypox: disease epidemiology, host immunity and clinical interventions. *Nat. Rev. Immunol.* **22**, 597–613 (2022).
4. Bunge, E. M. et al. The changing epidemiology of human monkeypox-A potential threat? A systematic review. *PLoS Negl. Trop. Dis.* **16**, e0010141 (2022).
5. Agency. UHS. Guidance: monkeypox: background information, (2022).
6. Organization, W. H. et al. *Monkeypox fact sheet*, (2024).
7. Zumla, A. et al. Monkeypox outbreaks outside endemic regions: scientific and social priorities. *Lancet Infect. Dis.* **22**, 929–931 (2022).
8. Titanji, B. K., Tegomoh, B., Nematollahi, S., Konomos, M. & Kulkarni, P. A. Monkeypox: A Contemporary Review for Healthcare Professionals. *Open Forum Infect. Dis.* **9**, ofac310 (2022).
9. Happi, C. et al. Urgent need for a non-discriminatory and non-stigmatizing nomenclature for monkeypox virus. *PLoS Biol.* **20**, e3001769 (2022).
10. Jia, H. et al. Genomic and epidemiological perspectives on the first local sporadic cases of Mpox in China. *Emerg. Microbes Infect.* **12**, 2245932 (2023).
11. Chi L., Zhang X., Xue Y. & Chen H. fastHaN: a fast and scalable program for constructing haplotype network for large-sample sequences. *Mol. Ecol. Resour.* https://doi.org/10.1111/1755-0998. 13829 (2023).
12. Isidro, J. et al. Phylogenomic characterization and signs of microevolution in the 2022 multi-country outbreak of monkeypox virus. *Nat. Med* **28**, 1569–1572 (2022).
13. Firth, C. et al. Using time-structured data to estimate evolutionary rates of double-stranded DNA viruses. *Mol. Biol. Evol.* **27**, 2038–2051 (2010).
14. Hammarlund, E. et al. Multiple diagnostic techniques identify previously vaccinated individuals with protective immunity against monkeypox. *Nat. Med* **11**, 1005–1011 (2005).
15. Luna, N. et al. Phylogenomic analysis of the monkeypox virus (MPXV) 2022 outbreak: emergence of a novel viral lineage? *Travel Med Infect. Dis.* **49**, 102402 (2022).
16. Reynolds, M. G. & Damon, I. K. Outbreaks of human monkeypox after cessation of smallpox vaccination. *Trends Microbiol* **20**, 80–87 (2012).
17. Kempe, C. H. et al. The use of vaccinia hyperimmune gamma-globulin in the prophylaxis of smallpox. *Bull. World Health Organ* **25**, 41–48 (1961).
18. Belyakov, I. M. et al. Shared modes of protection against poxvirus infection by attenuated and conventional smallpox vaccine viruses. *Proc. Natl Acad. Sci. USA* **100**, 9458–9463 (2003).
19. Moss, B. Smallpox vaccines: targets of protective immunity. *Immunol. Rev.* **239**, 8–26 (2011).
20. Li, M. et al. Three neutralizing mAbs induced by MPXV A29L protein recognizing different epitopes act synergistically against orthopoxvirus. *Emerg. Microbes Infect.* **12**, 2223669 (2023).

21. Meng, N. et al. Screening, expression and identification of nanobody against monkeypox virus A35R. *Int J. Nanomed.* **18**, 7173–7181 (2023).

22. Ren, Z. et al. Identification of mpox M1R and B6R monoclonal and bispecific antibodies that efficiently neutralize authentic mpox virus. *Emerg. Microbes Infect.* **13**, 2401931 (2024).

23. Gilchuk, I. et al. Cross-neutralizing and protective human antibody specificities to poxvirus infections. *Cell* **167**, 684–694.e689 (2016).

24. Zhang, R. R. et al. Rational development of multicomponent mRNA vaccine candidates against mpox. *Emerg. Microbes Infect.* **12**, 2192815 (2023).

25. Hooper, J. W., Custer, D. M. & Thompson, E. Four-gene-combination DNA vaccine protects mice against a lethal vaccinia virus challenge and elicits appropriate antibody responses in nonhuman primates. *Virology* **306**, 181–195 (2003).

26. Su, H. P., Golden, J. W., Gittis, A. G., Hooper, J. W. & Garboczi, D. N. Structural basis for the binding of the neutralizing antibody, 7D11, to the poxvirus L1 protein. *Virology* **368**, 331–341 (2007).

27. Liu J. et al. An efficient and safe trans-complementation system for MPXV mimicking authentic viral infection. *bioRxiv* https://doi.org/10.1101/2023.12.29.573498 (2023).

28. Chen, Z. et al. Chimpanzee/human mAbs to vaccinia virus B5 protein neutralize vaccinia and smallpox viruses and protect mice against vaccinia virus. *Proc. Natl Acad. Sci. USA* **103**, 1882–1887 (2006).

29. Esqueda A. et al. A monoclonal antibody produced in glycoengineered plants potently neutralizes monkeypox virus. *Vaccines (Basel)* **11**, 1179 (2023).

30. Wolffe, E. J., Vijaya, S. & Moss, B. A myristylated membrane protein encoded by the vaccinia virus L1R open reading frame is the target of potent neutralizing monoclonal antibodies. *Virology* **211**, 53–63 (1995).

31. Su H. et al. potent bispecific neutralizing antibody targeting glycoprotein B and the gH/gL/pUL128/130/131 complex of human cytomegalovirus. *Antimicrob Agents Chemother* **65**, e02422–20 (2021).

32. Zhou, B. et al. A bispecific broadly neutralizing antibody against enterovirus 71 and coxsackievirus A16 with therapeutic potential. *Antivir. Res* **161**, 28–35 (2019).

33. Schaefer, W. et al. Immunoglobulin domain crossover as a generic approach for the production of bispecific IgG antibodies. *Proc. Natl Acad. Sci. USA* **108**, 11187–11192 (2011).

34. Kaever, T. et al. Potent neutralization of vaccinia virus by divergent murine antibodies targeting a common site of vulnerability in L1 protein. *J. Virol.* **88**, 11339–11355 (2014).

35. Huang, B. et al. Isolation and characterization of monkeypox virus from the first case of monkeypox - chongqing municipality, China, 2022. *China CDC Wkly.* **4**, 1019–1024 (2022).

36. Tang, D. et al. Recombinant proteins A29L, M1R, A35R, and B6R vaccination protects mice from mpox virus challenge. *Front. Immunol.* **14**, 1203410 (2023).

37. Xia, A. et al. Cross-reactive antibody response to Monkeypox virus surface proteins in a small proportion of individuals with and without Chinese smallpox vaccination history. *BMC Biol.* **21**, 205 (2023).

38. Aldaz-Carroll, L. et al. Epitope-mapping studies define two major neutralization sites on the vaccinia virus extracellular enveloped virus glycoprotein B5R. *J. Virol.* **79**, 6260–6271 (2005).

39. Ravanello, M. P. & Hruby, D. E. Conditional lethal expression of the vaccinia virus L1R myristylated protein reveals a role in virion assembly. *J. Virol.* **68**, 6401–6410 (1994).

40. Hooper, J. W., Custer, D. M., Schmaljohn, C. S. & Schmaljohn, A. L. DNA vaccination with vaccinia virus L1R and A33R genes protects mice against a lethal poxvirus challenge. *Virology* **266**, 329–339 (2000).

41. Foo, C. H. et al. Vaccinia virus L1 binds to cell surfaces and blocks virus entry independently of glycosaminoglycans. *Virology* **385**, 368–382 (2009).

42. Bisht, H., Weisberg, A. S. & Moss, B. Vaccinia virus l1 protein is required for cell entry and membrane fusion. *J. Virol.* **82**, 8687–8694 (2008).

43. Benhnia, M. R. et al. Heavily isotype-dependent protective activities of human antibodies against vaccinia virus extracellular virion antigen B5. *J. Virol.* **83**, 12355–12367 (2009).

44. Zeng, Y. et al. The assessment on cross immunity with smallpox virus and antiviral drug sensitivity of the isolated mpox virus strain WIBP-MPXV-001 in China. *Emerg. Microbes Infect.* **12**, 2208682 (2023).

45. Benhnia, M. R. et al. Vaccinia virus extracellular enveloped virion neutralization in vitro and protection in vivo depend on complement. *J. Virol.* **83**, 1201–1215 (2009).

46. Appleyard, G., Hapel, A. J. & Boulter, E. A. An antigenic difference between intracellular and extracellular rabbitpox virus. *J. Gen. Virol.* **13**, 9–17 (1971).

47. Reynoso, G. V., Shannon, J. P., Americo, J. L., Gibbs, J. & Hickman, H. D. Growth and purification of vaccinia virus stocks for MPM imaging. *Methods Mol. Biol. (Clifton, NJ)* **2023**, 287–299 (2019).

48. Gibson, D. G. et al. Enzymatic assembly of DNA molecules up to several hundred kilobases. *Nat. Methods* **6**, 343–345 (2009).

49. McCoy, A. J. et al. Phaser crystallographic software. *J. Appl Crystallogr* **40**, 658–674 (2007).

Acknowledgements

Author contributions

G.C. and J.G. conceived and designed the study. G.C., J.G., X.W. and Y.Q. wrote and revised the manuscript. Y.Q., J.G., W.T., W.X., E.M., Q.J. M.F., and C.T. performed most of the experiments. Y.L and J.L. helped with the experiments. Y.Q. and J.G. analyzed the data. All the authors reviewed, critiqued, and provided comments on the text.

Competing interests

Patent applications have been filed that cover some of the antibodies presented here. GC, YQ, and WC are inventors. The other authors declare no competing interests.

Additional information

Supplementary information The online version contains supplementary material available at https://doi.org/10.1038/s41467-025-58180-z.

Correspondence and requests for materials should be addressed to Jiwan Ge or Gong Cheng.

Peer review information *Nature Communications* thanks Pavlo Gilchuk, who co-reviewed with Iuliia GilchukDimuthu Angage and the other, anonymous, reviewer(s) for their contribution to the peer review of this work. A peer review file is available.

Reprints and permissions information is available at http://www.nature.com/reprints

Publisher's note Springer Nature remains neutral with regard to jurisdictional claims in published maps and institutional affiliations.